All-Thin-Film Perovskite/C-Si Four-Terminal Tandems – Interlayer and Intermediate Contacts Optimization

Manuel Chapa*, Miguel F. Alexandre, Manuel J. Mendes*, Hugo Águas, Elvira Fortunato, Rodrigo Martins

i3N/CENIMAT, Department of Materials Science, Faculty of Science and Technology, Universidade NOVA de Lisboa and CEMOP/UNINOVA, Campus de Caparica, 2829-516 Caparica, Portugal

**Corresponding authors: m.chapa@campus.fct.unl.pt; mj.mendes@fct.unl.pt*

Abstract

Combined perovskite/crystalline-silicon 4-Terminal tandem solar cells promise >30% efficiencies. Here we propose all-thin-film double-junction architectures where high-bandgap perovskite top cells are coupled to ultra-thin c-Si bottom cells enhanced with light-trapping. A complete optoelectronic model of the devices was developed and applied to determine the optimal intermediate layers, which are paramount to maximize the cells' photocurrent. It was ascertained that, by replacing the transparent conductive oxides by grid-based metallic contacts in the intermediate positions, the parasitic absorption is lowered by 30%. Overall, a 29.2% efficiency is determined for ~2um thick tandems composed of the optimized interlayers and improved with Lambertian light-trapping.

Keywords: *Photovoltaics, Four-Terminal Double-Junction Solar Cells, Perovskite/Si Tandems, Light Trapping, Transparent Contacts.*

In recent years, the photovoltaic (PV) market has grown hastily due to rising adoption in emergent countries.[1] This has resulted in PV becoming one of the fastest growing industries, and the fastest growing energy source worldwide.[1,2] As a result, the installed PV capacity has grown from under 50 GW to above 400 GW in a matter of 7 years (2010 to 2017).[1]

Thin-film photovoltaics have been discussed as a potential high impact market, which could accompany the progress and growth of mobile electronics.[3] The need for reliable sources of power that can be integrated into mobile electronics by being flexible/bendable makes the research and development of PV technologies very enticing. Currently, this technology is still in a research stage, and thus it has yet to gain significant market attraction. The main aspects that are focused for such applications are the power density and mechanical properties (i.e. flexibility). Here, these challenges are tackled through the development of the design of multi-junction thin-films solar cells improved with light trapping.

This work focuses on perovskite/silicon four-terminal (4T) tandem solar cells for flexible applications. While other perovskite-based tandem architectures have been investigated with different bottom-cell materials (e.g. CIGS)[4], the market dominance of silicon and its favorable optical coupling with wide-bandgap perovskites makes the perovskite/silicon approach highly promising. The need for maximum power point (MPP) operation in the aforementioned applications encouraged the use of a 4T architecture in detriment of the common 2T architecture.[5,6] Considering the example of rooftop or utility-scale PV implementations, the angle and position of the solar cell should be such that the power output is maximized during assembly. On the other hand, mobile implementations do not benefit from these types of considerations, because the solar cells are used in a completely different manner. In the latter case, the solar

cell will be irradiated with a constantly varying amount of solar radiation and, therefore, 2T cells would be significantly limited by the series current. As such, we aim to study and optimize the most identifiable part of a 4T device, which is the interlayer. This serves as an electrical decoupler between the top and bottom cells and should simultaneously allow for maximum transmittance between themselves[7,8].

Furthermore, tandem 4T cells also require intermediate transparent contacts for charge collection as well as allowing light to reach the bottom cell. Traditionally, with TCOs, the overall manufacturing cost is increased, and device's performance is limited due to parasitic absorption.[7,9] As such, in addition to the interlayer optimization, we present here a study of transparent metallic-based contacts in the intermediate positions *in lieu* of ITO, in order to compare the optical performance of both types of intermediate contacts. Recently, nano- and micro-structured metallic contacts have seen increasing interest in the scientific community as an alternative to the industry standard ITO.[10] The replacement of ITO with these novel transparent electrodes is interesting in flexible PV, as they promise to be cheaper to implement, show high transmittance in the red and NIR region (where ITO strongly interacts with the incident radiation), better stress resistance/mechanical properties and do not pose sustainability issues as indium does.[10–12] Moreover, the recent application of micro-structured metallic contacts in both perovskite/silicon tandem solar cells and in single-junction PSCs has also revealed to bring additional optical enhancing effects in the devices[13,14].

While optoelectronic modelling of standard photovoltaic materials and architectures has been thoroughly reported and extensively studied,[15,16] novel materials, such as hybrid organic-inorganic perovskites (HOIPs) used in this work, have yet to see much modelling research. This can be chiefly attributed to several abnormal behaviors observed in these materials, such as the J-V hysteresis (i.e. the J-V dependence on the direction/speed of the bias scan), that casts doubts pertaining to their charge transport properties,[17] making their optoelectronic behavior nebulous when compared to standard inorganic materials such as c-Si. Nonetheless, it has been observed that charge transport in bulk perovskite can be accurately modeled by approximating it to an inorganic semiconductor, even presenting properties resembling those of GaAs[17]. In view of this, in the present work we adapt an existing model based on the drift-diffusion and Poisson equations, which is the basis of operation of the commercial software package *Lumerical Inc* DEVICE, to simulate the device's output. Such complete optoelectronic model, capable of tackling the study of tandem solar cells composed of virtually any type of sub-cells, revealed to be a particularly successful simulation approach in the optimization of perovskite/silicon double-junctions.

The analyzed device structure is shown in Fig. 1, for the two cases of intermediate transparent contacts based on either novel metallic arrays (i-TM) or TCOs (i-TCO). The tandem is comprised of a state-of-the-art 0.5 μm thick perovskite top cell coupled with an ultra-thin 1.5 μm c-Si bottom cell, in order to allow device flexibility and lower material costs. To optically model the metal-contacts variant (i-TM) we consider that the mesh has no interaction with the incident light, i.e. that the open areas between the metal fingers are much larger than the simulation volume, in order to avoid restricting the study to any particular contact geometry among the wide range of current possibilities (e.g. nanowire grids[18], fingers[19], honeycomb micro-meshes[12], etc.).

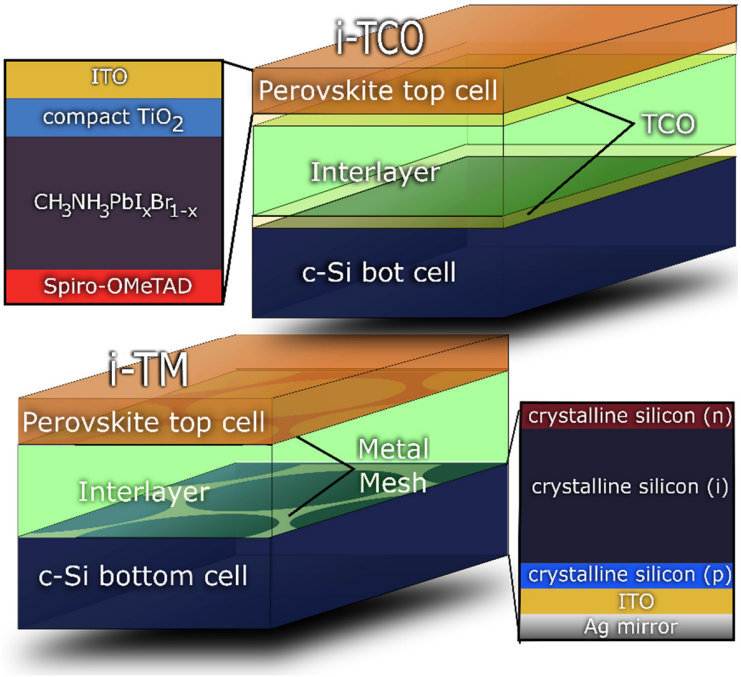

Figure 1: Sketches of the two 4-terminal (4T) double-junction solar cell architectures considered cases in the study. In the i-TM case (bottom), transparent metal contacts are considered in the intermediate positions bordering the interlayer; while in the i-TCO case (top), 100 nm thick ITO layers are considered in these contacts.

A wide-bandgap (1.75 eV) perovskite was taken for the top cell, for optimum pairing with c-Si, as calculated by Bremner and Levy.[20] The complex refractive index spectrum of the wide-bandgap HOIP considered in the simulations was adapted from the standard spectrum of 1.57 eV bandgap HOIP by blue-shifting the imaginary component by 0.18 eV. This is in accordance with recent experimental findings on higher band-gap perovskites that agree with a complete blue-shift of the real and imaginary parts of the refractive index, as utilized here and previously by Saliba et al.,[21,22] as well as supported by the Kramers-Kronig relation in which a variation of the absorption spectra of a material is accompanied by a variation in the refractive index. This is further described in the Supplementary Information (SI), accompanied by the remaining optical properties of the materials considered in the simulations.

An optimization procedure was performed, with the interlayer refractive index and thickness used as variables, for both i-TCO and i-TM cases of Fig. 1. The interlayer material is taken to be optically lossless in the relevant spectral range, so a real-valued refractive index is considered. In the i-TCO case, two ITO layers are located below and above the interlayer, as sketched in Fig. 1; while in the i-TM case there is no separation between the interlayer and the depicted layer structures of the top and bottom cells, given that the open spaces of the metal grid are considered sufficiently wide to neglect the effects of such grid in the cells' optical response. This is a reasonable approximation, since state-of-the-art transparent metallic contacts (metallic grids, fingers, nanowire arrays) can display red-NIR transmittance values around 90%[10].

We focus here on the silicon bottom cell performance. As a perovskite top cell is considered with a significant thickness (500 nm), the absorption of this layer needs little improvement, although thinner perovskite films could be considered when considering LT, as recently shown in literature.[23] As such, we seek to optimize the interlayer region for the benefit of the bottom cell, c-Si, and thus the photocurrent density of this layer is the chosen figure of merit.

Figures 2 a) and b) show the photocurrent density (J_{ph}) values attained in the Si bottom sub-cell for the different tandem configurations, and Table 1 lists the optimal interlayer parameters that yield the maximum

J_{ph}. In the i-TM case, the silicon absorption is higher than in the i-TCO case. Furthermore, a wider range of refractive index values, from 1.6 to 2.8, are usable for the i-TM. This observed range stems from the refractive indexes of the layers bordering the interlayer, i.e. spiro-OMeTAD at the top and c-Si at the bottom,[24,25] with the best interlayer index lying at 2.13 and thickness of 81 nm – corresponding to an index matching situation. In the i-TCO case, it is seen that low index values (below 1.6) are those that provide the highest absorbance metrics in silicon, resulting in a photocurrent maximum at an index of 1.36 and thickness of 213 nm. Given that ITO shows an index around 1.8 in the red-NIR region (lowering to 1.5 only at 1100 nm), it is observed that the optimization procedure in the i-TCO case did not converge to the expected index matching situation. This occurs due to an impromptu light-trapping mechanism taking place in the ITO/interlayer/ITO interfaces, making a low refractive index of the interlayer more desirable than a value closer to ITO. A schematic of the proposed light path mechanisms is shown in Fig. 2c) and d). The presence of a lower index medium in between the TCO layers establishes an "optical well" where the longer-wavelength light reflected from the bottom cell gets confined via multiple reflections occurring at the top and bottom surfaces of the interlayer. The light waves propagating back and forth in the interlayer are preferentially transmitted to the underneath high-index Si medium, due to its higher mode density, thus leading to the increase of the absorption of such otherwise lost NIR photons. The reasoning behind this is that the photon flux that reaches the bottom cell is at its highest in an index-matching case (in a planar scenario). Nonetheless, as the absorption coefficient of silicon is low for > 700 nm wavelengths, this does not directly lead to the highest light absorption. In fact, having a lower-index interlayer results in higher optical path lengths (thereby improved absorption probability) for the transmitted photons to the bottom cell due to the multiple reflection effect depicted in Fig. 2b. This counteracts and surpasses the increased reflection at the TCO/Low-index interlayer interface, i.e., the optical gains in the bottom cell attained with this effect surpass the optical losses at shorter red-NIR wavelengths from the use of a non-matched interlayer.

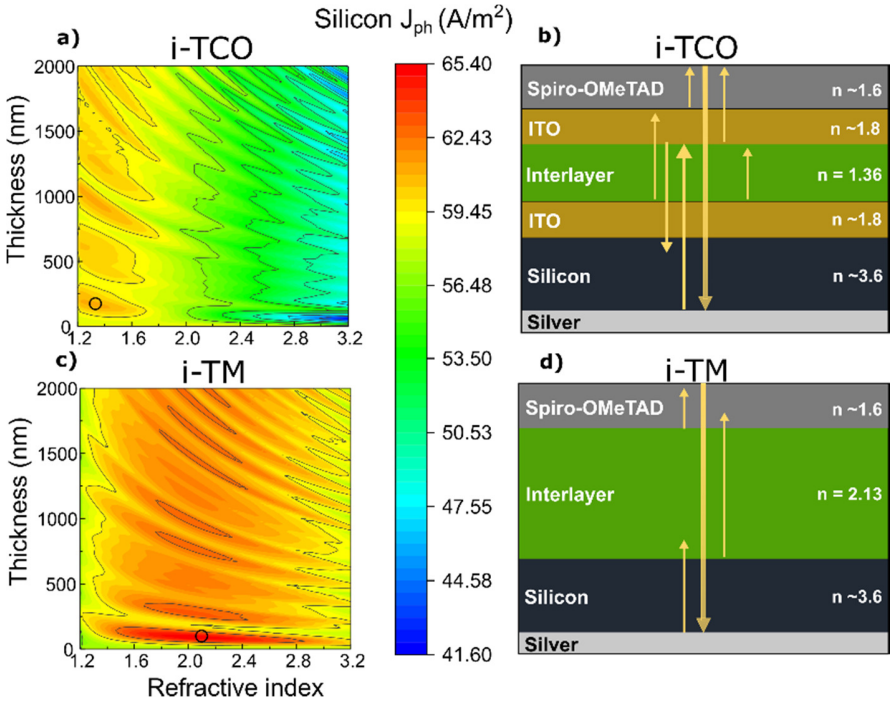

Figure 2: a), c) Contour plots describing the bottom c-Si cell's photocurrent density, J_{ph}, as a function of the interlayer's refractive index and thickness for the intermediate TCO contacts case (i-TCO) and for the intermediate transparent metal contacts case (i-TM), respectively; b) proposed light path mechanism for the i-TCO case, explaining the convergence to low refractive index values for the interlayer; d) index matching situation occurring in the optimized i-TM interlayer. The values where the maximum J_{ph} is verified are highlighted by a black circle.

The results of Fig. 2 indicate that different interlayer materials should be used in each intermediate contacts scenario. For the i-TCO architecture, some fluorinate polymers or UV-curable resins can be found with indexes as low as 1.31[26]. Higher indices, as preferable for the i-TM scenario, can be achieved by embedding high-index nanoparticles such as TiO_2 in the previous materials, and tuning the concentration of embedded particles to achieve the desired optical density.
Overall, the i-TM case shows a 30% decrease in parasitic absorption when compared to the standard i-TCO case, as the ITO equivalent absorption dropped by almost 50% (Table 1). In Supplementary Information it is also shown that the red and NIR reflection (700-1100 nm) for this design is 6.2% higher. Interestingly, this reflection increase is accompanied by a 6.9% increase in the maximum bottom cell photocurrent, leading to the ultimate conclusion that the bottom c-Si cell is nearing the absorption limit for the considered 1.5 μm thickness.

To solve these shortcomings, advanced light trapping (LT) techniques can be used to increase the device's optical performance, for instance by forward scattering incident light to a range of angles away from the incidence direction, in order to increase its optical path length (OPL) inside the absorber material[23,27]. This optical process leads to a similar behavior to that of simply increasing the c-Si film thickness. To acquire a general view of the benefits resulting from light management techniques, the Lambertian light trapping limits were calculated for the bottom cell (Fig. 3b)). These correspond to the maximum LT enhancements that can be achieved and analytically determined within the conceptual regime of ray optics.[28–30] Integrating the solar spectrum in the 700-1100 nm range (i.e. the intended absorption region for the bottom cell), the maximum J_{ph} is found to be 233.3 A/m^2. The analytical data presented in Fig. 3 a) shows that a 30 μm cell with ideal *Lambertian* LT lead to a J_{ph} of 228.9 A/m^2. It is therefore logical that, for thicknesses > 30 μm, the observed theoretical photocurrent gains are minimal. These observations indicate that thin c-Si cells may be in fact ideal for the bottom absorber role, as the reduced thicknesses means higher carrier collection efficiency, because the cell's thickness starts approaching the carrier diffusion lengths leading to a lower recombination.

Table 1: Summary of the equivalent spectrally-integrated absorption, represented by the calculated J_{ph}, occurring in the layers composing the tandem structure with the indicated optimal interlayer parameters, for both the i-TCO and i-TM cases.

	i-TCO	**i-TM**
Materials	**J_{ph} (A/m^2)**	
ITO	16.06	8.27
Compact TiO_2	0.89	2.28
HOIP	221.70	216.77
Spiro-OMeTAD	5.58	6.42
c-Si	61.13	65.37
Total (tandem)	305.52	299.13
Optimal interlayer parameters		
Refractive index, *n*	1.36	2.13
Thickness (nm)	160	81

In what concerns the J_{ph} values (i.e. integrated absorption) for the perovskite top cell shown in Table 1 for both cases, it is notable that its performance also depends on the interlayer(s) parameters. This is due to the longer-wavelength tail of the extinction coefficient of the perovskite material (see Fig. S1) which causes a

small absorption of the light reflected from the underlying layers and bottom cell, as seen by the NIR peaks in the perovskite absorption spectra of Fig. 3.

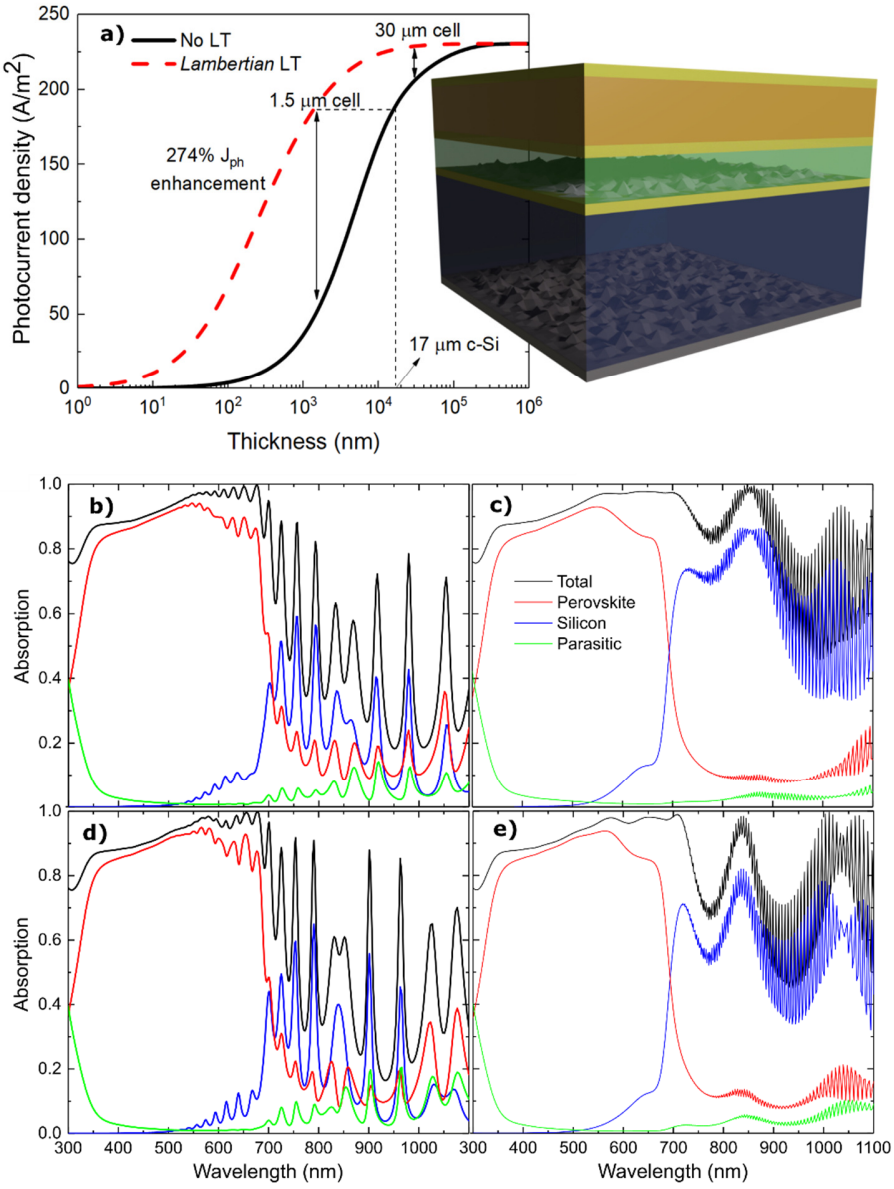

Figure 3: a) Lambertian light trapping (LT) limits for a range of c-Si thickness values of the bottom cell, considering the AM1.5 illumination spectrum only within 700-1100 nm wavelength range. It is shown that the LT-enhanced 1.5 µm thick cell reaches a photocurrent equal to that of a planar (without LT) cell having 17 µm c-Si thickness. The inset is an illustrative schematic of Lambertian light trapping applied to the bottom cell of a four-terminal double-junction. b-e) Absorption spectra in the tandem device considering the i-TM (b,c) and i-TCO (d,e) cases with 1.5 µm (b,d) and 17 µm (c,e – equivalent to LT-enhanced 1.5 µm) c-Si thickness.

Considering the aforementioned methodology to test the effects of light trapping on the silicon bottom cell, the absorption spectra were determined for both the i-TM and i-TCO designs, using a 1.5 and 17 µm silicon optical thickness (Fig. 3 c), e)). As expected, in the i-TM design, the silicon bottom cell is not as hindered by parasitic absorption as in the i-TCO case.

In what concerns the modelling of the I-V response of the devices, common inorganic semiconductor solar cells can be accurately described using the drift-diffusion formalism that neglects hot electron and quantum effects, because the motion in these materials mostly behaves in a classical manner[17,31]. However, such considerations do not entirely hold in the case of perovskite materials. As explained earlier, this is not only due to anomalous observed behaviors (i.e. J-V hysteresis), but also as a consequence of the device's heterojunction architecture. Specifically, the mathematical formalism employed by the numerical solver (drift-diffusion equations) can break down with sharply varying electric fields – an intrinsic characteristic of heterojunctions as those in PSCs (at ETL/Perovskite and Perovskite/HTL). However, even though the charge-transport mechanisms in hybrid-perovskites can be influenced by their organic parts, they can be modelled by approximating it to an all-inorganic semiconductor. The same logic is applicable to the organic spiro-OMeTAD, where the hole-separating role of this material is modeled through parameters that may not directly match those of the material.[32] The compact TiO_2 and ITO parameters were sourced from the literature in similar fashion,[32] while the parameters for c-Si were directly used from the software's database. All the physical parameters considered are presented in SI.

The resulting IV curves are shown in Fig. 4 and the main parameters are summarized in Table 2. Here it can be seen that the PSC has a 20.49% efficiency figure, slightly lower than a state-of-the art 1.57 eV PSC.[33] This is expectable for a higher bandgap cell, as the bandgap starts to deviate from the optimum single-junction value at around 1.5 eV.[20] Finally, we then see combined device efficiencies for the tandem higher than the record Si performance[34]. This is in accordance with recent studies that predict up-to 31.6% efficiencies for these tandem devices[19].

When a planar (without LT) approach was studied, there was a similar performance between both designs, associated with the lower c-Si thickness that was complemented by a rather insubstantial parasitic absorption and effect of the index matching. Only here, by emulating light-trapping techniques, we see the fruits of the labor that was the interlayer optimization and the ITO replacement, resulting in the 9% lower total reflection and 8% higher c-Si absorption for I-TM, when compared to I-TCO.

With the performance shifting in favor of the bottom cell, the main parasitic absorbers (ITO and spiro-OMeTAD) started showing a less unwanted absorbed radiation. A difference between the absorptions of the ITO and spiro-OMeTAD layers is still noted between the architectures, where the i-TM, understandably, presents less than half the parasitic ITO absorption of the I-TCO due to the eliminated contacts. These layers, particularly the organic spiro-OMeTAD, persist as a substitution priority in perovskite architectures, partly due to the parasitic absorption exhibited by either and the degradation potential presented by the organic layer. Alternatives for hole-transport materials have been searched in the organics and oxides alike – and even the removal of the HTL has been considered -, and further studies should be made in this area.[35,36]

Following these conclusions, further numerical simulations were performed where the optical thickness of the c-Si was varied (within the calculated limits of 1.5 to 17 μm, Fig. 3), while the thickness used for electrical simulations was kept constant at 1.5 μm. The associated results are summarized in Table 2, and the simulated IV curve of the top performing design is shown in Fig. 4.

Comparing both LT cases, it is seen that besides of a higher efficiency, both cases show increased open circuit voltage (V_{oc}), which can be directly related to higher rate of carrier generation resultant of the LT emulation. As more carriers are being photogenerated while maintaining the thickness (from an electrical point of view), the fill-factor increases as expected, due to a consequently higher conversion and collection rate.

Table 2: Main quantities of the 1-Sun J-V characteristics of the various optical path lengths of the silicon cell, for both the i-TM and i-TCO cases. The planar cases consider 1.5 µm c-Si bottom cells without LT, while the LT-enhanced cases consider c-Si cells having a red-NIR absorption equivalent to a 17 µm thick c-Si absorber, in accordance with the Lambertian analysis (Fig. 3 a)).

		Case	V_{OC} (V)	J_{sc} (A/m²)	FF (%)	Eff. (%)
i-TM architecture	**Si bottom cell**	Planar	0.57	33.6	82.00	1.57
		LT	0.60	153.3	83.29	7.73
	Perovskite top cell	Planar	1.25	215.9	84.87	23.01
		LT	1.25	200.9	85.07	21.46
i-TCO architecture	**Si bottom cell**	Planar	0.56	30.5	82.00	1.42
		LT	0.60	138.8	83.22	6.96
	Perovskite top cell	Planar	1.25	220.5	84.76	23.48
		LT	1.25	204.8	85.03	21.87

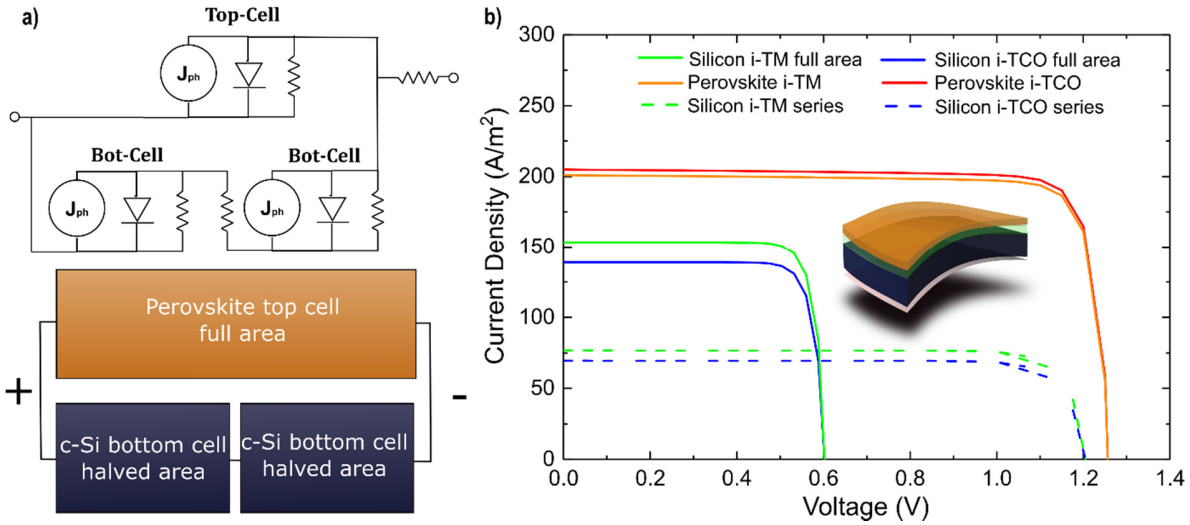

Figure 4: a) Schematic and equivalent electric circuit of the proposed tandem unit cell, composed by a perovskite top cell coupled in parallel to two series-connected Si bottom cells with half area. b) output JV curves of the top perovskite cell (red i-TCO, orange i-TM) and bottom c-Si cell (blue i-TCO, green i-TM), with both the full area (full line) and series configuration (dashed line) represented.

In summary, it is concluded that the i-TM design benefited from both higher optical matching and lower parasitic absorption, thus leading to a better performance than its counterpart (Fig. 5). This study also showed the benefits of light trapping methods as means to improve the bottom cell absorption, thus emphasizing an important and inexpensive way to obtain high efficiency 4T tandem cells. Most notably, in the i-TM case, we see that a silicon bottom cell of an equivalent optical thickness of 17 µm allows for an overall conversion efficiency of 29.19% when coupled with a high-bandgap perovskite top cell.

The model developed shows great promise in aiding the design and optimization of multijunction devices such as the ones presented in this work. The modelling of the perovskite cell, in particular, is a great step in the further integration of this novel technology into the photovoltaic industry, where the prediction of the optoelectronic behavior of the device is of great importance.

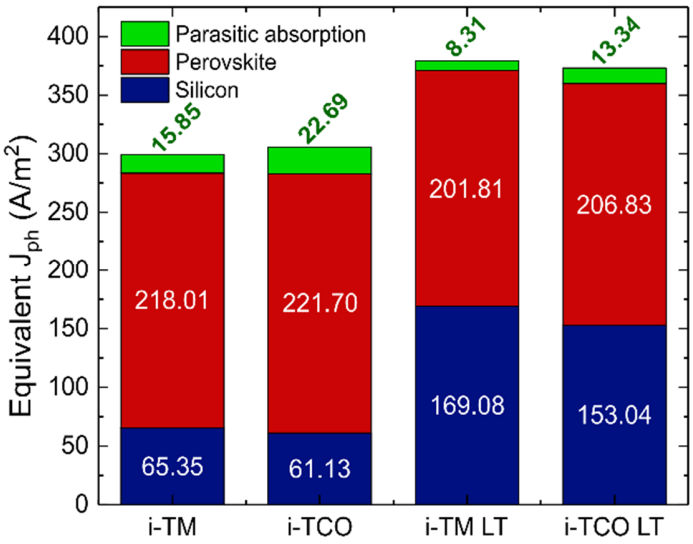

Figure 5: Summary bar plot showing the calculated photocurrent density (i.e. integrated absorption spectrum) within the Perovskite (Top cell), c-Si (Bottom cell) and remaining materials (Parasitic), for the two cases (i-TCO and i-TM) of intermediate contacts analyzed in this work, as well as with and without the implementation of Lambertian light-trapping (LT).

Supplementary Information

Contains the details concerning the materials' properties that were used for the modelling procedures, and simulated reflection spectra of the considered devices. Also, a description of the procedure used for blue shifting the optical properties of the perovskite material is present.

Author contributions

M. C. devised the modelling setup, performed the simulations and wrote the manuscript. M. F. A. assisted in developing the optoelectronic model and revised the results and manuscript. M. J. M. projected the work, discussed the results and revised the manuscript. E.F., H.A. and R.M. revised the manuscript and supervised the work and financing projects.

Acknowledgements

This work was funded by FEDER funds, through the COMPETE 2020 Program, and national funds, through the Portuguese Foundation for Science and Technology (FCT-MEC), under the projects POCI-01-0145-FEDER-007688 (Reference UID/CTM/50025), ALTALUZ (Reference PTDC/CTM-ENE/5125/2014), SuperSolar (PTDC/NAN-OPT/28430/2017) and TACIT (PTDC/NAN-OPT/28837/2017). M. J. Mendes acknowledges funding by FCT-MEC through the grant SFRH/BPD/115566/2016.

References

(1) Michael Schmela; SolarPower Europe. Global Market Outlook For Solar Power: 2018 - 2022. **2018**, 1–81.

(2) International Energy Agency. *World Energy Balances*, 1st ed.; IEA Publications, 2018.

(3) Vicente, A. T.; Araújo, A.; Mendes, M. J.; Nunes, D.; Oliveira, M. J.; Sanchez-Sobrado, O.; Ferreira, M. P.;

Águas, H.; Fortunato, E.; Martins, R. Multifunctional Cellulose-Paper for Light Harvesting and Smart Sensing Applications. *J. Mater. Chem. C* **2018**, *6* (13), 3143–3181.

(4) Shen, H.; Duong, T.; Peng, J.; Jacobs, D.; Wu, N.; Gong, J.; Wu, Y.; Karuturi, S. K.; Fu, X.; Weber, K.; et al. Mechanically-Stacked Perovskite/CIGS Tandem Solar Cells with Efficiency of 23.9% and Reduced Oxygen Sensitivity. *Energy Environ. Sci.* **2018**, *11* (2), 394–406.

(5) Phillips, L. J.; Rashed, A. M.; Treharne, R. E.; Kay, J.; Yates, P.; Mitrovic, I. Z.; Weerakkody, A.; Hall, S.; Durose, K. Maximizing the Optical Performance of Planar CH 3 NH 3 PbI 3 Hybrid Perovskite Heterojunction Stacks. *Sol. Energy Mater. Sol. Cells* **2016**, *147*, 327–333.

(6) Chen, B.; Bai, Y.; Yu, Z.; Li, T.; Zheng, X.; Dong, Q.; Shen, L.; Boccard, M.; Gruverman, A.; Holman, Z.; et al. Efficient Semitransparent Perovskite Solar Cells for 23.0%-Efficiency Perovskite/Silicon Four-Terminal Tandem Cells. *Adv. Energy Mater.* **2016**, *6* (19), 1601128.

(7) Werner, J.; Barraud, L.; Walter, A.; Bräuninger, M.; Sahli, F.; Sacchetto, D.; Tétreault, N.; Paviet-Salomon, B.; Moon, S. J.; Allebé, C.; et al. Efficient Near-Infrared-Transparent Perovskite Solar Cells Enabling Direct Comparison of 4-Terminal and Monolithic Perovskite/Silicon Tandem Cells. *ACS Energy Lett.* **2016**, *1* (2), 474–480.

(8) Hajjiah, A.; Parmouneh, F.; Hadipour, A.; Jaysankar, M.; Aernouts, T. Light Management Enhancement for Four-Terminal Perovskite-Silicon Tandem Solar Cells: The Impact of the Optical Properties and Thickness of the Spacer Layer between Sub-Cells. *Materials (Basel).* **2018**, *11* (12), 2570.

(9) Lyubchyk, A.; Vicente, A.; Alves, P. U.; Catela, B.; Soule, B.; Mateus, T.; Mendes, M. J.; Aguas, H.; Fortunato, E.; Martins, R. Influence of Post-Deposition Annealing on Electrical and Optical Properties of ZnO-Based TCOs Deposited at Room Temperature. *Phys. status solidi* **2016**, *12*, 1–12.

(10) Sannicolo, T.; Lagrange, M.; Cabos, A.; Celle, C.; Simonato, J.-P.; Bellet, D. Metallic Nanowire-Based Transparent Electrodes for Next Generation Flexible Devices: A Review. *Small* **2016**, *12* (44), 6052–6075.

(11) Afshinmanesh, F.; Curto, A. G.; Milaninia, K. M.; Van Hulst, N. F.; Brongersma, M. L. Transparent Metallic Fractal Electrodes for Semiconductor Devices. *Nano Lett.* **2014**, *14* (9), 5068–5074.

(12) Torrisi, G.; Luis, J. S.; Sanchez-Sobrado, O.; Raciti, R.; Mendes, M. J.; Águas, H.; Fortunato, E.; Martins, R.; Terrasi, A. Colloidal-Structured Metallic Micro-Grids: High Performance Transparent Electrodes in the Red and Infrared Range. *Sol. Energy Mater. Sol. Cells* **2019**, *197* (March), 7–12.

(13) Ma, T.; Song, Q.; Tadaki, D.; Niwano, M.; Hirano-Iwata, A. Unveil the Full Potential of Integrated-Back-Contact Perovskite Solar Cells Using Numerical Simulation. *ACS Appl. Energy Mater.* **2018**, *1* (3), 970–975.

(14) Adhyaksa, G. W. P.; Johlin, E.; Garnett, E. C. Nanoscale Back Contact Perovskite Solar Cell Design for Improved Tandem Efficiency. *Nano Lett.* **2017**, *17* (9), 5206–5212.

(15) Mendes, M. J.; Araújo, A.; Vicente, A.; Águas, H.; Ferreira, I.; Fortunato, E.; Martins, R. Design of Optimized Wave-Optical Spheroidal Nanostructures for Photonic-Enhanced Solar Cells. *Nano Energy* **2016**, *26*, 286–296.

(16) Vicente, A. T.; Wojcik, P. J.; Mendes, M. J.; Águas, H.; Fortunato, E.; Martins, R. A Statistics Modeling Approach for the Optimization of Thin Film Photovoltaic Devices. *Sol. Energy* **2017**, *144*, 232–243.

(17) Brenner, T. M.; Egger, D. A.; Kronik, L.; Hodes, G.; Cahen, D. Hybrid Organic—inorganic Perovskites: Low-Cost Semiconductors with Intriguing Charge-Transport Properties. *Nat. Rev. Mater.* **2016**, 16011.

(18) Langley, D. P.; Giusti, G.; Lagrange, M.; Collins, R.; Jiménez, C.; Bréchet, Y.; Bellet, D. Silver Nanowire Networks: Physical Properties and Potential Integration in Solar Cells. *Sol. Energy Mater. Sol. Cells* **2014**, *125*, 318–324.

(19) Löper, P.; Moon, S.-J.; Martín de Nicolas, S.; Niesen, B.; Ledinsky, M.; Nicolay, S.; Bailat, J.; Yum, J.-H.; De Wolf, S.; Ballif, C. Organic–inorganic Halide Perovskite/Crystalline Silicon Four-Terminal Tandem Solar Cells. *Phys. Chem. Chem. Phys.* **2015**, *17* (3), 1619–1629.

(20) Bremner, S. P.; Levy, M. Y.; Honsberg, C. B. Analysis of Tandem Solar Cell Efficiencies under AM1.5G

Spectrum Using a Rapid Flux Calculation Method. *Prog. Photovoltaics Res. Appl.* **2008**, *16* (3), 225–233.

(21) McMeekin, D. P.; Sadoughi, G.; Rehman, W.; Eperon, G. E.; Saliba, M.; Horantner, M. T.; Haghighirad, A.; Sakai, N.; Korte, L.; Rech, B.; et al. A Mixed-Cation Lead Mixed-Halide Perovskite Absorber for Tandem Solar Cells. *Science (80-.).* **2016**, *351* (6269), 151–155.

(22) Werner, J.; Nogay, G.; Sahli, F.; Yang, T. C. J.; Bräuninger, M.; Christmann, G.; Walter, A.; Kamino, B. A.; Fiala, P.; Löper, P.; et al. Complex Refractive Indices of Cesium-Formamidinium-Based Mixed-Halide Perovskites with Optical Band Gaps from 1.5 to 1.8 EV. *ACS Energy Lett.* **2018**, *3* (3), 742–747.

(23) Haque, S.; Mendes, M. J.; Sanchez-, O.; Águas, H.; Fortunato, E.; Martins, R. Photonic-Structured TiO2 for High-Efficiency, Flexible and Stable Perovskite Solar Cells. *Nano Energy* **2019**.

(24) König, T. A. F.; Ledin, P. A.; Kerszulis, J.; Mahmoud, M. A.; El-Sayed, M. A.; Reynolds, J. R.; Tsukruk, V. V. Electrically Tunable Plasmonic Behavior of Nanocube–Polymer Nanomaterials Induced by a Redox-Active Electrochromic Polymer. *ACS Nano* **2014**, *8* (6), 6182–6192.

(25) Palik, E. D. *Handbook of Optical Constants of Solids*; Palik, E., Ed.; Academic Press: London, 1985.

(26) SpecialChem. Low & Ultra-low Refractive Index Polymers https://omnexus.specialchem.com/tech-library/article/low-ultra-low-refractive-index-polymers (accessed Apr 20, 2019).

(27) Alexandre, M.; Chapa, M.; Haque, S.; Mendes, M. J.; Águas, H.; Fortunato, E.; Martins, R. Optimum Luminescent Down-Shifting Properties for High Efficiency and Stable Perovskite Solar Cells (In Press). *ACS Appl. Energy Mater.* **2019**.

(28) Mendes, M. J.; Haque, S.; Sanchez-Sobrado, O.; Araújo, A.; Águas, H.; Fortunato, E.; Martins, R. Optimal-Enhanced Solar Cell Ultra-Thinning with Broadband Nanophotonic Light Capture. *iScience* **2018**, *3*, 238–254.

(29) Sanchez-Sobrado, O.; Mendes, M. J.; Haque, S.; Mateus, T.; Araujo, A.; Aguas, H.; Fortunato, E.; Martins, R. Colloidal-Lithographed TiO2photonic Nanostructures for Solar Cell Light Trapping. *J. Mater. Chem. C* **2017**, *5* (27), 6852–6861.

(30) Mendes, M. J.; Araújo, A.; Vicente, A.; Águas, H.; Ferreira, I.; Fortunato, E.; Martins, R. Design of Optimized Wave-Optical Spheroidal Nanostructures for Photonic-Enhanced Solar Cells. *Nano Energy* **2016**, *26*, 286–296.

(31) Datta, S. *Quantum Phenomena*, 1st ed.; Addison-Wesley Publishing Company: Reading, Massachusetts, 1989.

(32) Zhou, Q.; Jiao, D.; Fu, K.; Wu, X.; Chen, Y.; Lu, J.; Yang, S. Two-Dimensional Device Modeling of CH3NH3PbI3 Based Planar Heterojunction Perovskite Solar Cells. *Sol. Energy* **2016**, *123*, 51–56.

(33) Saliba, M.; Matsui, T.; Seo, J.-Y.; Domanski, K.; Correa-Baena, J.-P.; Nazeeruddin, M. K.; Zakeeruddin, S. M.; Tress, W.; Abate, A.; Hagfeldt, A.; et al. Cesium-Containing Triple Cation Perovskite Solar Cells: Improved Stability, Reproducibility and High Efficiency. *Energy Environ. Sci.* **2016**, *9* (6), 1989–1997.

(34) Holman, Z. C.; Descoeudres, a; De Wolf, S.; Ballif, C. Record Infrared Internal Quantum Efficiency in Silicon Heterojunction Solar Cells With Dielectric/Metal Rear Reflectors. *IEEE J. Photovoltaics* **2013**, *3* (4), 1243–1249.

(35) Watson, B. L.; Rolston, N. J.; Printz, A. D.; Dauskardt, R. H. Scaffold-Reinforced Perovskite Compound Solar Cells. *Energy Environ. Sci.* **2017**, 0–25.

(36) Yang, M.; Li, Z.; Reese, M. O.; Reid, O. G.; Kim, D. H.; Siol, S.; Klein, T. R.; Yan, Y.; Berry, J. J.; van Hest, M. F. A. M.; et al. Perovskite Ink with Wide Processing Window for Scalable High-Efficiency Solar Cells. *Nat. Energy* **2017**, *2* (5), 17038.